

Spin, charge, and orbital correlations in the one-dimensional t_{2g} -orbital Hubbard model

J. C. Xavier,^{1,2} H. Onishi,³ T. Hotta,³ and E. Dagotto¹

¹*Condensed Matter Sciences Division, Oak Ridge National Laboratory, Oak Ridge, TN 37831 and
Department of Physics, The University of Tennessee, Knoxville, TN 37996*

²*Universidade Estadual Paulista, CP 713, 17015-970 Bauru, SP, Brazil*

³*Advanced Science Research Center, Japan Atomic Energy Research Institute, Tokai, Ibaraki 319-1195, Japan
(Dated: July 20, 2005)*

We present the zero-temperature phase diagram of the one-dimensional t_{2g} -orbital Hubbard model, obtained using the density-matrix renormalization group and Lanczos techniques. Emphasis is given to the case for the electron density $n=5$ corresponding to five electrons per site, of relevance for some Co-based compounds. However, several other cases for electron densities between $n=3$ and 6 are also studied. At $n=5$, our results indicate a first-order transition between a paramagnetic (PM) insulator phase and a fully-polarized ferromagnetic (FM) state by tuning the Hund's coupling. The results also suggest a transition from the $n=5$ PM insulator phase to a metallic regime by changing the electron density, either via hole or electron doping. The behavior of the spin, charge, and orbital correlation functions in the FM and PM states are also described in the text and discussed. The robustness of these two states varying parameters suggests that they may be of relevance in more realistic higher dimensional systems as well.

PACS numbers: 75.30.kz, 71.10.Fd, 75.50.Cc, 75.10.-b

I. INTRODUCTION

The study of the exotic properties of cobalt oxides is an area of investigations that is currently attracting considerable attention in the research field of condensed matter physics. Among the main reasons for this wide effort, the recent discovery of superconductivity in layered two-dimensional triangular lattices of Co atoms with the composition Na_xCoO_2 has certainly triggered a rapid increase of research activities on cobalt oxides. This material becomes superconducting after H_2O is intercalated,¹ opening an exciting area of investigations.

The experimentally unveiled phase diagram of this compound varying the Na composition has revealed the existence of several other competing tendencies: Charge ordered as well as magnetic states are stabilized, in addition to superconductivity.² In the related compound $(\text{Ca}_2\text{CoO}_3)(\text{CoO}_2)$, a spin incommensurate spin-density-wave has been recently reported.³ The existence of such a rich phase diagram is a characteristic of strongly correlated electron systems, where complex behavior typically emerges due to the presence of competing states that have similar energies but vastly different transport and magnetic properties.⁴

Additional motivation for the study of Co-oxides arises from recent experimental studies of hole-doped cobaltites in the perovskite form such as $\text{La}_{1-x}\text{Sr}_x\text{CoO}_3$, where clear tendencies toward phase separation between ferromagnetic (FM) metallic and paramagnetic (PM) insulating regions have been found.⁵ This establishes an intriguing qualitative connection between Co-oxides and the famous manganites that exhibit the colossal magnetoresistance, effect widely believed to originate in an analogous mixed-phase tendency exhibited by Mn-oxides.⁶ In fact, a large magnetoresistance in some cobaltites has

also been observed, and its origin appears related with phase competition.⁷ As a consequence, establishing the dominant ground-state tendencies of simple models for cobaltites is important to envision the possible phase mixtures that may lead to exotic behavior.

As a third motivation for the study of cobaltites, it is known that some Co-based compounds have interesting thermoelectric properties. In particular, a huge thermoelectric power has been recently discovered in NaCo_2O_4 by Terasaki *et al.*,⁸ opening another area of investigations, with a focus on thermoelectric materials mainly with the purpose of industrial applications.

For all these reasons, the theoretical study of models for Co-oxides is timely and needed in order to guide further experimental developments. Ab-initio calculations have already provided important information in this context,⁹ and the inclusion of many-body effects is the natural next step. Previous theoretical studies of Co-based systems including Coulombic repulsion have mainly focused on triangular lattices. In this context, recent Monte Carlo investigations unveiled the presence of magnetic correlations.¹⁰ Fluctuation-exchange approximations also revealed tendencies toward ferromagnetism and possible triplet-pairing instabilities in a multiorbital model.¹¹ Several approximate studies of t - J ¹² and single-band Hubbard models¹³ have also been presented.

To understand the behavior of complex oxides, it is of particular importance the analysis of the many possible tendencies in the ground state, namely the study of the various competing states stabilized as electron density and coupling are modified. Unfortunately, this task is difficult due to a lack of reliable unbiased analytical techniques. For this reason, the first effort toward a detailed numerical analysis of models for cobaltites is presented here. Instead of directly emphasizing the triangu-

lar lattice with approximate techniques or exactly studying small systems, we have preferred to perform a systematic study of a one-dimensional multiorbital Hamiltonian, exploring in detail the coupling and electron density parameter space, and using computationally exact techniques. This level of accuracy is achieved through the use of reliable methods such as the density-matrix renormalization group (DMRG)¹⁴ and the Lanczos technique.¹⁵ We envision this effort as a first step toward a systematic computational analysis of more complicated quasi-two-dimensional triangular-lattice systems.

The paper is organized as follows. In Sec. II, the multiorbital model is introduced and many-body computational techniques used here are briefly discussed. In Sec. III, the main results are presented. These results are organized based on the observable studied: First, the $n=5$ phase diagram is discussed, where n denotes the number of electron per site. Then, the spin correlations are presented at several values of n . This is followed by the charge and orbital correlations. Finally, conclusions are presented in Sec. IV. The main result of the paper is the clear dominance of two rather different ground states: (1) a FM state and (2) a PM state with short-range correlations. Both are very robust varying couplings and densities. Their higher-dimensional versions may be of relevance for present and future Co-oxide experiments.

II. MODEL AND TECHNIQUE

In the investigation reported in this manuscript, we consider a three-orbital Hubbard model, defined on a one-dimensional chain along the x -axis with L sites. The three orbitals represent the t_{2g} orbitals of relevance for cobaltites. The model is given by

$$\begin{aligned}
 H = & - \sum_{j,\gamma,\gamma',\sigma} t_{\gamma,\gamma'} \left(d_{j,\gamma\sigma}^\dagger d_{j+1,\gamma'\sigma} + \text{H.c.} \right) \\
 & + U \sum_{j,\gamma} \rho_{j,\gamma\uparrow} \rho_{j,\gamma\downarrow} + \frac{U'}{2} \sum_{j,\sigma,\sigma',\gamma \neq \gamma'} \rho_{j,\gamma\sigma} \rho_{j,\gamma'\sigma'} \\
 & + \frac{J}{2} \sum_{j,\sigma,\sigma',\gamma \neq \gamma'} d_{j,\gamma\sigma}^\dagger d_{j,\gamma'\sigma'}^\dagger d_{j,\gamma\sigma'} d_{j,\gamma'\sigma} \\
 & + \frac{J'}{2} \sum_{j,\sigma \neq \sigma',\gamma \neq \gamma'} d_{j,\gamma\sigma}^\dagger d_{j,\gamma'\sigma'}^\dagger d_{j,\gamma'\sigma'} d_{j,\gamma\sigma}, \quad (1)
 \end{aligned}$$

where the index j denotes the site of the chain, γ indicates the orbitals xy , yz , and zx , and σ is the spin projection along the z -axis. The rest of the notation is standard. The hopping amplitudes are $t_{xy,xy}=t_{zx,zx}=t=1$, and zero for the other cases. These simple values for the hopping amplitudes can be easily derived from the overlap of d_{xy} , d_{yz} , and d_{zx} orbitals between nearest-neighbor sites along the x -axis. The interaction parameters U , U' , J , and J' are the standard ones for multiorbital Hamiltonians, and a detailed description can be found in Ref. 6. These couplings are not independent, but they satisfy the

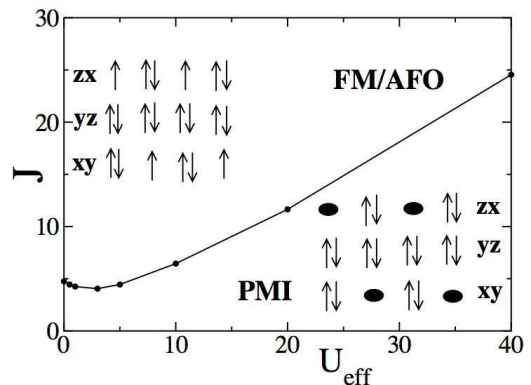


FIG. 1: Ground-state phase diagram for the one-dimensional three-orbital Hubbard model, using a 6-site chain and working at electron density $n=5$. FM and PMI denote the regions with ferromagnetism and paramagnetism (insulator), respectively. We also present a schematic picture of the electron configurations. AFO indicates the staggered population of orbitals in the FM state. The reader should consult the text for more details, as well as the next figure.

well-known relations $J'=J$ and $U=U'+2J$, due to the reality of the wave function and the rotational symmetry in the orbital space.

We investigate the model described above mainly using the DMRG technique with open boundary conditions.¹⁴ The finite-size algorithm is employed for sizes up to $L=48$, keeping up to $m=350$ states per block. The truncation errors are kept around 10^{-5} or smaller. The center blocks in our DMRG procedure are composed of 64 states due to the three orbitals. Note that, for instance, the t - J model has only 3 states in these center blocks. As a consequence, keeping $m=350$ states per block in the t_{2g} -orbital Hubbard model is analogous to keeping $m \sim 7000$ states per block in the t - J model.

Although in related investigations specific values of U and J for the triangular Co-oxides were discussed,¹¹ here we prefer to vary independently these couplings analyzing the possible ground states that are stabilized by this procedure. In fact, the ratio U/J may change among the many interesting Co-oxides, and in addition, it is important to classify the states that could be stabilized by the proper isovalent chemical doping, external fields, or perturbations.

III. RESULTS

A. Phase diagram for density $n=5$

In Fig. 1, the ground-state phase diagram J versus $U_{\text{eff}}=U'-J$ is presented. For large J , a fully polarized FM phase is obtained, while for small J , a PM regime is found. This PM phase is insulating, as shown below. Note that the phase diagram is obtained by comparing

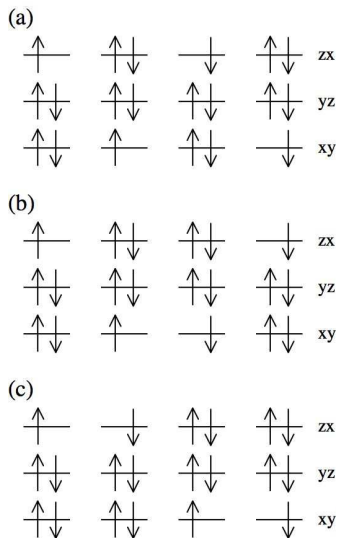


FIG. 2: States with the largest weight in the ground state of a 4-site chain solved exactly. Note that each state has 8-fold degeneracy. At $J=0$, these three states have the same weight. On the other hand, for nonzero J , the state (a) (and its 8-fold degenerate states) has the largest weight, with a spin (orbital) structure factor peaked at $\pi/2$ (π). The states (b) and (c) (each one also with degeneracy 8) have the second- and third-largest weights, respectively, for nonzero J .

the energies for different sectors of the z -projection of the total spin, S_{total}^z , mainly using a system of size $L=6$. Other values of L are also studied, and it is observed that for $L=4, 6, 8$, and 10 , in the PM regime the ground state has total spin $0, 1, 0$, and 1 , respectively, for a large set of couplings investigated. As a consequence, it is reasonable to assume that the transition line separates states with the minimum and maximum total spin, without intermediate partially polarized regimes. The phase diagram we have found has similarities with that already reported by two of the authors at density $n=4$,¹⁶ in the context of spin-1 chains.

As described later, our results for the spin-spin, charge-charge, and orbital correlations suggest, roughly, an electron distribution at short distances, as schematically presented in Fig. 1. The electron configuration in the FM phase is quite simple: 5 electrons per site, with a polarized net spin $1/2$ and antiferro-orbital (AFO) correlations. The existence of FM correlations is a direct consequence of the multiorbital nature of the model and the robust value of J in the FM regime.

On the other hand, a more complex electron configuration emerges in the PM phase. The meaning of the full circles in the inset of Fig. 1 for the PM phase is to denote either a spin up or a spin down. Note, however, that quantum fluctuations are strong and the configuration shown in Fig. 1 is just a guidance. To obtain insight into the ground-state wave function, it is useful to consider the case of a four-site chain, where results can be

obtained exactly by using the Lanczos method. In the strong-coupling limit $U_{\text{eff}} \gg J \gg 1$ (or, more precisely, $1/(U' - J) \ll 1$), it is found that the most important portion of the ground-state wave function is expressed as

$$|\psi\rangle = \frac{1}{\sqrt{24}} \sum_{\mathbf{P}} (-1)^{n_{\mathbf{P}}} \times \left(\begin{array}{c} \uparrow\downarrow \\ \uparrow\downarrow \\ \downarrow \end{array} \right) \otimes \left(\begin{array}{c} \downarrow \\ \uparrow\downarrow \\ \uparrow\downarrow \end{array} \right) \otimes \left(\begin{array}{c} \uparrow\downarrow \\ \uparrow\downarrow \\ \uparrow \end{array} \right) \otimes \left(\begin{array}{c} \uparrow \\ \uparrow\downarrow \\ \uparrow\downarrow \end{array} \right), \quad (2)$$

where the sum is taken over the permutation of the four spinors and $n_{\mathbf{P}}$ is the number of permutation we have to perform to recover the original configuration. Namely, the electron configuration presented in the PM phase of Fig. 1 should be regarded as the equivalent of the 4 spinors contained in $|\psi\rangle$. Note that this is not a rigid configuration, but all permutations are equally important at small J . In particular, all the 24 states have the same weight in the ground state at $J=0$, while at finite J , the 24 states are split into three classes with 8 states for each, as shown in Fig. 2. Note that each of these classes lead to a distinct peak position in the spin and orbital structure factors. When the peak positions in these channels are denoted by q_{spin} and q_{orbital} , the class (a) has $q_{\text{spin}}=\pi/2$ and $q_{\text{orbital}}=\pi$, class (b) $q_{\text{spin}}=\pi/2$ and $q_{\text{orbital}}=\pi/2$, and class (c) $q_{\text{spin}}=\pi$ and $q_{\text{orbital}}=\pi/2$. The yz orbital is fully occupied due to the one dimensionality of the system that prevents the movement of electrons in this orbital due to a vanishing hopping. For the active xy and zx orbitals, the electrons are not distributed in a rigid charge-ordered pattern, but instead the density is to an excellent approximation equal to 1.5 at every site. Note that a similar representation of the ground-state wave function for four sites has been found for the $SU(4)$ spin-orbital model.¹⁷ As discussed in more detail below, these two models are related to each other.

B. Spin correlations at several densities

To understand more quantitatively the magnetic order present in the PM phase, it is useful to measure the spin-spin correlation function, defined as

$$C_{\text{spin}}(l) = \frac{1}{M} \sum_{|i-j|=l} \langle S_i^z S_j^z \rangle, \quad (3)$$

where $S_i^z = \sum_{\gamma} (\rho_{i\gamma\uparrow} - \rho_{i\gamma\downarrow})/2$ is the z -projection of the total spin at each site and M is the number of site pairs (i, j) satisfying $l=|i-j|$. We average over all pairs of sites separated by distance l , in order to minimize boundary effects. In Fig. 3(a), $C_{\text{spin}}(l)$ is shown for the PM phase. It is found that the numerical data of $C_{\text{spin}}(l)$ are well reproduced by the function

$$\tilde{C}_{\text{spin}}(j) = \frac{a}{j^2} + b \frac{\cos(\frac{\pi}{2}j)}{j^{3/2}}, \quad (4)$$

as shown by the dashed curve. Note that a and b are appropriate fitting parameters. The result indicates that the spin-spin correlation function has a four-site periodicity and decays as a power law with critical exponent $3/2$. In the inset of Fig. 3(a), we also present the Fourier transform of the spin-spin correlation function,

$$S(q) = \frac{1}{L} \sum_{j,k} e^{iq(j-k)} \langle S_j^z S_k^z \rangle, \quad (5)$$

for $L=16$ and $L=48$. As observed in this figure, finite-size effects appear to be very small. Here we clearly find a peak in $S(q)$ at $q=\pi/2$, corresponding to the four-site periodicity of the spin-spin correlation function.

Let us here discuss the physical meaning of the four-site periodicity. Since the yz orbital is fully occupied in our studies, the t_{2g} -orbital Hubbard model can be regarded as a two-orbital Hubbard model composed only of xy and zx orbitals. Note that for this two orbital model, the hopping amplitudes are symmetric and there is no off-diagonal elements. Moreover, when $J=0$, in the two orbital model, there exists an extra $SU(4)$ symmetry involving both spin and orbital degrees of freedom. In such a case, the effective Hamiltonian in the strong-coupling limit is given by the $SU(4)$ spin-orbital model, which has been investigated intensively in recent years.^{18,19,20} Concerning a less symmetric case than $SU(4)$, the effect of J has also been discussed,^{21,22} where anisotropic exchange interactions arise in the orbital part. Note that the spin-spin correlation function, presented in Fig. 3(a), is found to have a four-site periodicity and decay as a power law with critical exponent $3/2$.²³ These results are consistent with previous analytical work²⁴ and numerical analysis^{18,21} for the $SU(4)$ spin-orbital model.

Here we stress that the spin-spin correlation functions for $n=5$ clearly present distinct behavior from the results already reported at $n=4$,¹⁶ where an exponential decay has been observed, as depicted as a linear-log plot in Fig. 3(b). The result indicates a *gapless* spin-excitation spectrum for $n=5$, with power-law decaying correlations, in contrast to a gapfull behavior for $n=4$. Note that, for better comparison, we have normalized C_{spin} in such a way that the correlations are the same at distance one. We have eliminated the odd sites for $n=5$, since the results there are close to zero (see Fig. 3(a)). Note also that working with $m=350$, it is difficult to reach good accuracy for the correlations at large distances, since they are very small. For this reason, in our results we present only the first 19 sites.²⁵

In Fig. 3(b), we also show the spin-spin correlation function for $n=3$, reported here for the first time to our knowledge. In the case of $n=3$, it is naively expected that the local spin $S=3/2$ is formed at each site. By analogy with the half-odd-integer-spin antiferromagnetic Heisenberg chains, we expect the power-law decay of the spin-spin correlation function and a gapless spin-excitation spectrum as well.²⁶ On the contrary, we can observe in Fig. 3(b) that the spin-spin correlation function shows an exponential decay similar to the case for the integer-spin

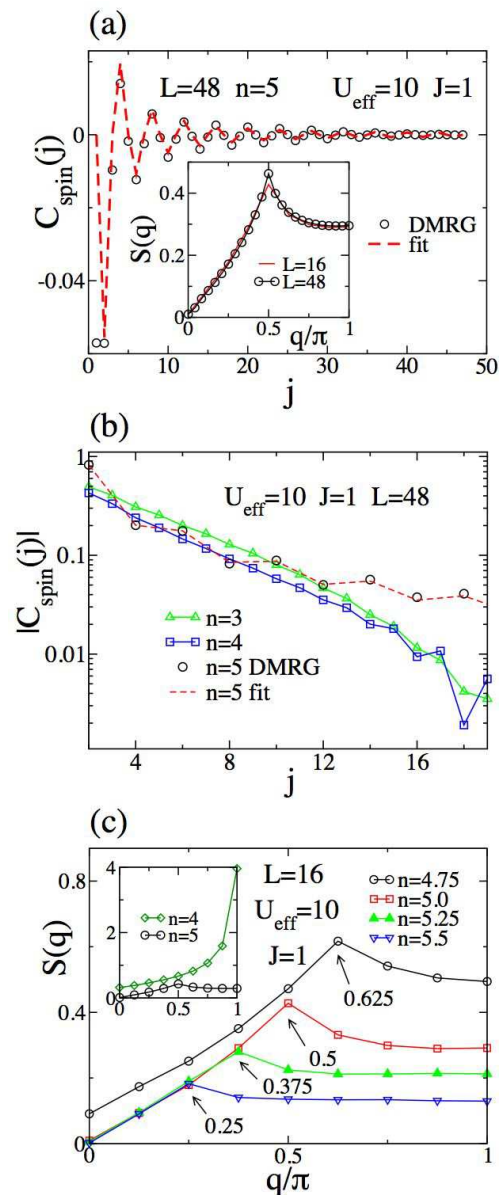


FIG. 3: (a) The spin-spin correlation function $C_{\text{spin}}(j)$ vs. j for $L=48$ and density $n=5$. The dashed line indicates a fit using Eq. (4). The inset shows the spin structure factor $S(q)$ for $L=16$ and $L=48$. (b) The linear-log plot of the module of the spin-spin correlation $|C_{\text{spin}}(j)|$ corresponding to densities $n=3, 4$, and 5 with $L=48$, as well as the fit used in (a). For details, see the main text. (c) Spin structure factor $S(q)$ for several densities n , and using $L=16$. The arrows indicate the peak positions. In all plots $U_{\text{eff}}=10$ and $J=1$, as indicated. Inset shows $S(q)$ for $n=4$ and 5 .

chains. To understand this peculiar behavior, it is necessary to take into account the effect of t_{2g} orbitals. As mentioned above, electrons in the yz orbital cannot hop, while electrons in the xy and zx orbitals move to adjacent sites with the same amplitude. Then, it is expected that only electrons in the xy and zx orbitals contribute to the

exchange interaction, and the $n=3$ system is regarded as an effective $S=1$ chain, leading to the exponential decaying spin-spin correlation function.

In Fig. 3(c), $S(q)$ is shown for several densities. Since the finite-size effects seem to be small, we consider $L=16$. As observed in these studies, the results suggest that the peak position changes linearly with the electron density as $q=(6-n)\pi/2 \pmod{\pi}$. Note that this peak is clearly robust for $n=4$, as shown in the inset of Fig. 3(c), and substantially decreases its intensity by increasing the density n .

It is important to remark that the inset of Fig. 3(a) is very similar to the results found by Ogata and Shiba in their study of the one-dimensional Hubbard model at quarter-filling and $U=\infty$ (see Fig. 9 of Ref. 27). Clearly, in the model studied in this paper, the electrons in the two bands with a nonzero hopping behave like one-band models with a strong on-site repulsion, at least from the perspective of the spin correlations. Note, however, that these two one-band models are connected via the Coulombic repulsion which, as discussed below, will open a gap in the spectrum of charge excitations.

C. Charge correlations at several densities

To investigate the charge excitations, it is useful to measure the charge gap, defined as $\Delta=E(N_e+2)+E(N_e-2)-2E(N_e)$, where $E(N_e)$ denotes the lowest energy in the subspace with the total number of electrons N_e . In Fig. 4(a), the charge gap is shown as a function of $1/L$ at densities $n=4$ and 5 , for particular values of U_{eff} and J . Clearly, at these densities the charge gap extrapolates to a nonzero value in the thermodynamic limit, indicating that the system is an *insulator*. On the other hand, as shown in Fig. 4(b), for non-integer electron densities, the charge gaps seem to extrapolate to zero in the thermodynamic limit, suggesting a metallic behavior. These results indicate that a transition from an insulating phase to a metallic regime is obtained by changing the density away from $n=5$.

In Fig. 4(c), the charge gap for the density $n=5$ and $L=12$ is presented. It appears that U' is the main driver of the system into an insulating phase. On the other hand, the Hund's coupling J has the opposite effect: As observed in Fig. 4(d), by increasing J the charge gap decreases. Note that U' plays a role similar to that of the nearest-neighbor Coulomb repulsion V in the two-leg ladder extended Hubbard model (with the two legs playing the role of the two orbitals in our model). In the ladder case, it is known that V drives the system to an insulator at quarter-filling.²⁸

We have also investigated the charge structure factor, defined as

$$N^{\gamma,\gamma'}(q) = \frac{1}{2L} \sum_{j,k} e^{iq(j-k)} \left(N^{\gamma,\gamma'}(j,k) + N^{\gamma',\gamma}(j,k) \right), \quad (6)$$

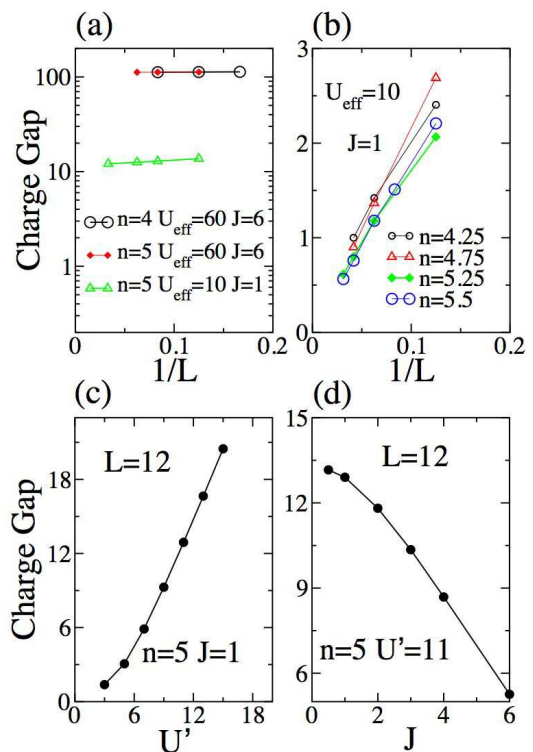


FIG. 4: (a) The charge gap Δ vs. $1/L$ at particular values of U_{eff} and J , and densities $n=4$ and $n=5$. (b) Same as (a) but for non-integer densities, and $U_{\text{eff}}=10$ and $J=1$. (c) and (d) denote the charge gap for density $n=5$ and $L=12$. (c) contains Δ vs. U' at $J=1$, while (d) shows Δ as a function of J at $U'=11$.

where $N^{\gamma,\gamma'}(j,k)=\langle \delta n_{\gamma}(j) \delta n_{\gamma'}(k) \rangle$ and $\delta n_{\gamma}(j)=n_{\gamma}(j) - \langle n_{\gamma}(j) \rangle$. In a periodic system $N^{\gamma,\gamma'}(j,k)=N^{\gamma',\gamma}(j,k)$. However, with open boundary conditions, as used in our investigation, this is not valid any more, due to the presence of Friedel oscillations. Using the definition discussed above, $N^{\gamma,\gamma'}(q=0)$ is always zero. In our calculations, we obtained $N^{\gamma,\gamma'}(q=0) < 10^{-4}$, indicating that we have retained enough states in the truncation process to satisfy this constraint.

The best indication of a true long-range-order (LRO) can be obtained by the system-size dependence of $N^{\gamma,\gamma'}(q)$. If $N^{\gamma,\gamma'}(q^*)/L \rightarrow \text{constant}$ as $L \rightarrow \infty$, at some particular q^* , a true LRO characterized by q^* is present. Carrying out this analysis, we have found no evidence of LRO in the charge sector of $n=5$. In Figs. 5(a), (c), and (e), typical examples of the charge structure factor for the FM and PM phases at density $n=5$ are presented. In the FM phase, we are able to explore very large system sizes, since we can measure the correlations in the sector of $S_{\text{total}}^z = \max$, with a much smaller Hilbert space than for the PM phase. Although we did not find LRO, the behavior of the structure factor suggests that in the FM phase the charge-charge correlation presents a quasi-LRO due to the presence of a robust peak at $q=\pi$. In fact, in

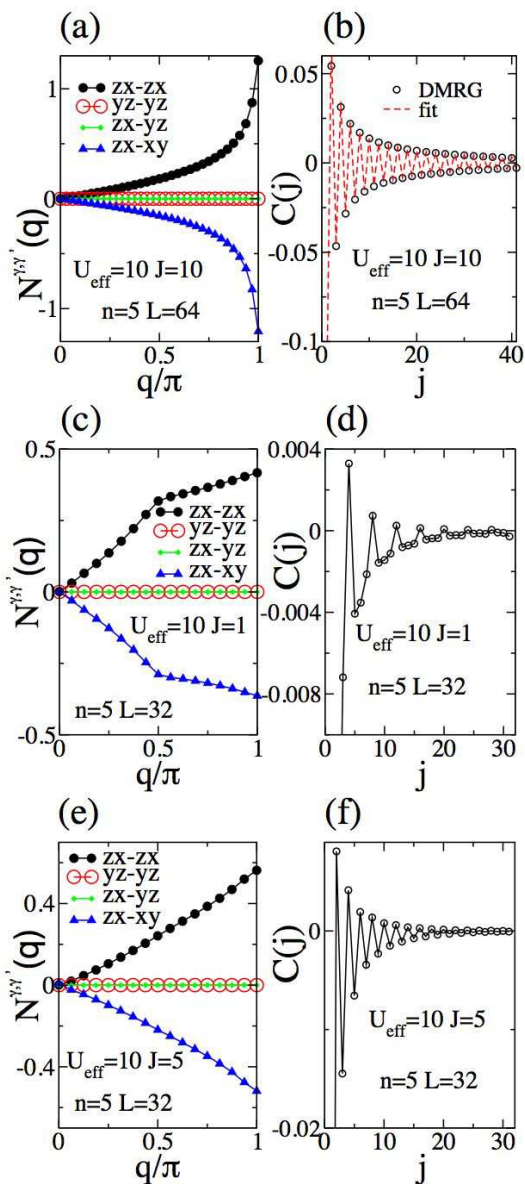


FIG. 5: The charge structure factor $N^{\gamma,\gamma'}(q)$ and the charge-charge correlation function $C(j)$, at density $n=5$. (a) and (b) are for $U_{\text{eff}}=10$, $J=10$ and $L=64$. This corresponds to the FM regime of Fig. 1. The dashed line is a fit using the function $a \cos(\pi j)/j$ with an appropriate fitting parameter a . (c) and (d) are for $U_{\text{eff}}=10$, $J=1$, and $L=32$. This is in the PM regime of Fig. 1. (e) and (f) are the same as (c) and (d), respectively, but for $J=5$.

the charge-charge correlation function, defined as

$$C(l) = \frac{1}{M} \sum_{|i-j|=l} \langle \delta n_{zx}(i) \delta n_{zx}(j) \rangle, \quad (7)$$

we observe a slow power-law decay, as shown in Fig. 5(b). This correlation oscillates as $\cos(\pi j)/j$, as indicated by the dotted curve in Fig. 5(b). The DMRG data agree very nicely with a fit using this function. These strong

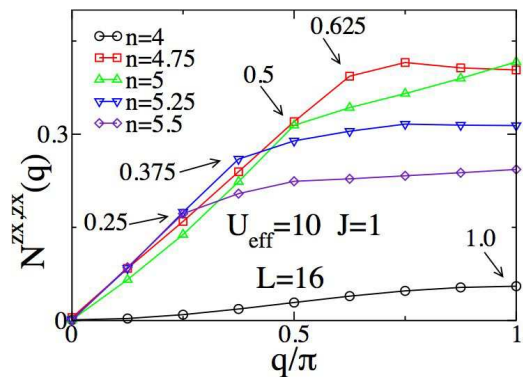


FIG. 6: The charge structure factor $N^{zx,zx}(q)$ for several densities and using $U_{\text{eff}}=10$, $J=1$, and $L=16$. The arrows indicate the cusp positions.

charge oscillations suggest that the system may develop LRO rapidly, when a coupling in the direction perpendicular to the chains is introduced. Then, spin-FM charge-ordered states should be seriously considered as a possibility for Co-oxide materials, although more detailed calculations are needed to confirm this speculation.

Note also that the negative values of $N^{zx,xy}(q = \pi)$ suggest an alternation of charge occupation between the zx and xy orbitals, as in the schematic representation in Fig. 1 (FM phase). Indeed, as discussed later in more detail, there is quasi-long-range AFO order. A similar result has already been found in the FM phase for the density $n=4$.¹⁶

On the other hand, in the PM phase, $N^{\gamma,\gamma'}(q)$ does not present a peak as sharp as for the FM phase, as shown in Fig. 5(c). In fact, the magnitude of the charge correlations is drastically different between the PM and FM phases, as can be seen from the absolute values of these correlations in the vertical axes of Figs. 5(b) and (d). Also note that the appearance of the cusp at $q=\pi/2$ is related to the four-site periodicity of the correlation $C(l)$, as shown in Fig. 5(d).

Our results also suggest that the charges behave differently in two distinct regimes in the PM phase. At small J , the correlation $C(l)$ presents a four-sites periodicity, while for larger J , only a two-site periodicity is found, as observed in Fig. 5(f). In addition, the cusp of $N^{zx,zx}(q)$ present in the small- J regime disappears at larger J (Fig. 5(e)), apparently continuously. We have also observed that at small J , the position of the cusp changes with the electron density in a similar way as $S(q)$, as shown in Fig. 6.

D. Orbital correlations at $n=5$

Consider now the possibility of orbital order. In the PM phase and for $n=5$, we have found that the xy and zx orbitals are those of relevance, since the yz orbitals are fully occupied. Note that in the PM phase and at

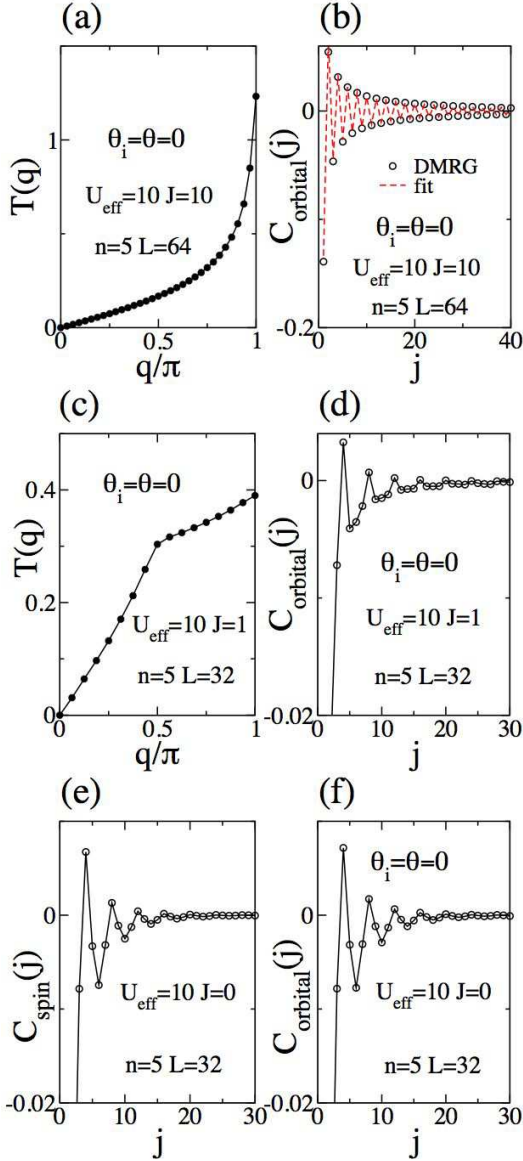


FIG. 7: (a) The orbital structure factor $T(q)$ versus momentum for $U_{\text{eff}}=10$, $J=10$, and $L=64$ with $\theta_i=\theta=0$. (b) The orbital correlation $C_{\text{orbital}}(j)$ for the same parameters as used in (a). The dashed line is a fit using the function $a \cos(\pi j)/j$. (c) and (d) are the same as (a) and (b), but for $U_{\text{eff}}=10$, $J=1$, and $L=32$. (e) and (f) contain the correlations $C_{\text{spin}}(j)$ and $C_{\text{orbital}}(j)$ for $U_{\text{eff}}=10$, $J=0$, and $L=32$. All the results are for the density $n=5$.

$n=4$, the orbital degree of freedom becomes inactive due to the ferro-orbital order.¹⁶ Then, here we take the pseudospin representation for the xy and zx orbitals, and measure the orbital correlations to determine the orbital structure. For this purpose, we introduce an angle θ_j to characterize the orbital shape at each site. Using the

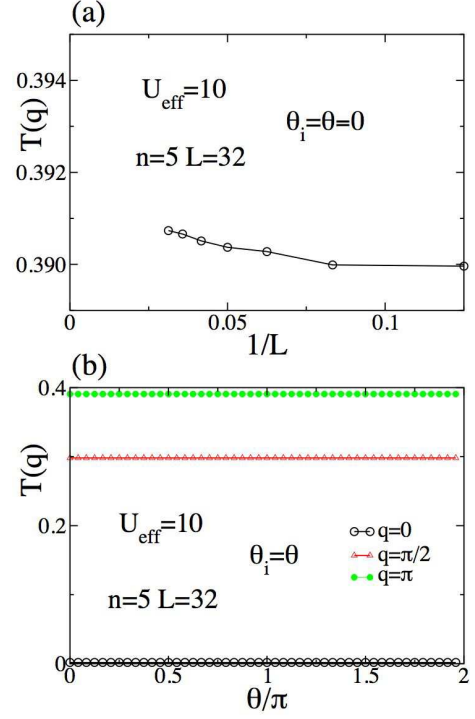


FIG. 8: (a) The size dependence of the orbital structure factor $T(q)$ at $q=\pi$ with $\theta_i=\theta=0$, at density $n=5$. (b) $T(q)$ vs. θ for particular values of q .

angle θ_j , we define the phase-dressed operators as

$$\begin{cases} f_{j,a,\sigma} = e^{i\theta_j/2} (\cos(\theta_j/2)d_{j,xy,\sigma} + \sin(\theta_j/2)d_{j,zx,\sigma}), \\ f_{j,b,\sigma} = e^{i\theta_j/2} (-\sin(\theta_j/2)d_{j,xy,\sigma} + \cos(\theta_j/2)d_{j,zx,\sigma}). \end{cases} \quad (8)$$

The optimal orbitals, a and b , are determined so as to maximize the orbital structure factor, defined by

$$T(q) = \frac{1}{L} \sum_{j,k} e^{iq(j-k)} \langle T^z(i)T^z(j) \rangle, \quad (9)$$

where $T^z(j) = \sum_{\sigma} (f_{j,a,\sigma}^{\dagger} f_{j,a,\sigma} - f_{j,b,\sigma}^{\dagger} f_{j,b,\sigma})/2$.

Let us first focus on the case $\theta_i=\theta=0$. In Figs. 7(a) and (c), typical examples of the orbital structure factor in the FM and PM phases at density $n=5$ are presented. Note that these results are similar to those of the charge structure factor shown in Figs. 5(a) and (c), as previously anticipated. Also, as shown in Figs. 7(b) and (d), concerning the orbital correlation function defined as

$$C_{\text{orbital}}(l) = \frac{1}{M} \sum_{|i-j|=l} \langle T^z(i)T^z(j) \rangle, \quad (10)$$

we find the same form as $C(l)$, as observed in Figs. 5(b) and (d). In the FM phase, as shown in Fig. 7(b), $C_{\text{orbital}}(l)$ decays as $\cos(\pi j)/j$, which is the signature of quasi-long-range AFO. On the other hand, in the PM phase, we observe a four-site periodicity of $C_{\text{orbital}}(j)$ as well as that of $C_{\text{spin}}(j)$, while the peak position of $T(q)$

is at $q=\pi$ for $U_{\text{eff}}=10$ and $J=1$. Note that the spin-spin correlation function shows the four-site periodicity and $S(q)$ has the peak at $q=\pi/2$ for $U_{\text{eff}}=10$ and $J=1$, as shown in Fig. 3(a).

To clarify the similarity between the two-orbital model composed of the xy and zx orbitals and the $SU(4)$ spin-orbital model, we investigate $C_{\text{spin}}(l)$ and $C_{\text{orbital}}(l)$ for the present t_{2g} model, at $U_{\text{eff}}=10$ and $J=0$. As shown in Figs. 7(e) and (f), it is clearly observed that $C_{\text{orbital}}(l)$ and $C_{\text{spin}}(l)$ present exactly the same behavior with a four-site periodicity, due to the presence of the $SU(4)$ symmetry at $J=0$. When we include the effect of J , the spin and orbital degrees of freedom are no longer equivalent, but we can observe the four-site periodicity in both $C_{\text{orbital}}(l)$ and $C_{\text{spin}}(l)$ due to the influence of the $SU(4)$ symmetry at $J=0$. Thus, the short-range orbital correlation for small J originates in the $SU(4)$ singlet at $J=0$.

It should be mentioned that there is no indication of orbital LRO in the PM phase, since $T(\pi)$ converges to a finite value in the thermodynamic limit, as shown in Fig. 8(a). On the other hand, although we have found no signature of orbital order between the xy and zx orbitals through the orbital structure factor $T(q)$ for $\theta_i=\theta=0$, a more complex combination between these orbitals could exist, but we cannot observe it directly from $T(q)$ with $\theta=0$. In order to consider other combinations, we set $\theta_i=\theta$ and change the value of θ . However, even in this case, we do not observe any changes in $T(q)$, as observed in Fig. 8(b). Namely, the orbital correlation does not change due to the rotation in the orbital space, and we cannot determine the optimal orbitals. Note that even if we optimize θ_i at each site, $T(\pi)$ is always maximum. Thus, we conclude that the states considered in our investigations do not have long-range orbital order in the PM phase.

IV. CONCLUSIONS

In this paper, we have investigated the properties of the one-dimensional Hubbard model with three active orbitals, with emphasis on electron densities of relevance for cobalt oxides. We envision this work as a first step toward a numerical accurate study of many-body Hamiltonians for Co-oxides including the Coulombic repulsion. Our main result is the identification of two dominant tendencies in the ground state. For example, at sufficiently

large Hund's coupling, a tendency toward a fully saturated ferromagnetic state exists. This state may develop long-range charge order in the case when the interorbital repulsion U' is large, at density $n=5$, and for nonzero values of the coupling in the direction perpendicular to the chains.

In previous investigations of Co-oxides models, tendencies toward FM were also discussed (see, for instance, Refs. 10 and 11 and references therein). Thus, evidence is accumulating that magnetic states should be of relevance for these materials. This is clearly compatible with experiments for perovskites cobaltites.⁵ However, thus far only for large Na doping, magnetism has been observed experimentally in triangular lattices.² This result may arise from the competition with the higher dimensional version of the PM state discussed in this work. This state has short-range correlations in all channels, and in some limits it has an extra $SU(4)$ symmetry as in two orbital models. While this exact symmetry may appear only in one dimension and for $J=0$, remnants may remain under more realistic conditions.

To the extent that our results can be qualitatively extended to higher dimensions, the main competition in Co-oxide models originates from FM and PM states, with long-range and short-range spin and charge order, respectively. Of course, the effect of geometrical frustration could be also an important ingredient to bring about the complex spin-charge-orbital structure in the triangular-lattice systems. In fact, two of the authors have revealed that the spin frustration is suppressed due to the orbital ordering in the e_g -orbital model on a zigzag chain.²⁹ In addition, in the present work we have identified metal-insulator transitions with doping away from $n=5$, while the main properties in the spin and charge sectors remain similar as for the integer density $n=5$. The next challenge is to increase the dimensionality of the t_{2g} system toward two dimensions by studying ladders and/or zigzag chains. Work is in progress in this direction.

Acknowledgments

This work was supported by DMR-0454504 (E. D. and J. C. X.) and FAPESP-04/09689-2 (J. C. X.). T. H. is supported by the Japan Society for the Promotion of Science and by the Ministry of Education, Culture, Sports, Science, and Technology of Japan.

¹ K. Takada, H. Sakurai, E. Takayama-Muromachi, F. Izumi, R. A. Dilanian, and T. Sasaki, *Nature* **422**, 53 (2003); R. E. Schaak, T. Klimczuk, M. L. Foo, and R. J. Cava, *Nature* **424**, 527 (2003).

² Y. Wang, N. S. Rogado, R. J. Cava, and N. P. Ong, *Nature* **423**, 425 (2003); T. Motohashi, R. Ueda, E. Naujalis, T. Tojo, I. Terasaki, T. Atake, M. Karppinen, and H. Ya-

mauchi, *Phys. Rev. B* **67**, 64406 (2003).

³ J. Sugiyama, H. Itahara, T. Tani, J. H. Brewer, and E. J. Ansaldo, *Phys. Rev. B* **66**, 134413 (2002); J. Sugiyama, J. H. Brewer, E. J. Ansaldo, B. Hitti, M. Mikami, Y. Mori, and T. Sasaki, *Phys. Rev. B* **69**, 214423 (2004).

⁴ E. Dagotto, *Complexity in Strongly Correlated Electronic Systems*, to appear in *Science*, 2005.

- ⁵ R. Caciuffo, D. Rinaldi, G. Barucca, J. Mira, J. Rivas, M. A. Senaris-Rodriguez, P. G. Radaelli, D. Fiorani, and J. B. Goodenough, Phys. Rev. B **59**, 1068 (1999); P. L. Kuhns, M. J. R. Hoch, W. G. Moulton, A. P. Reyes, J. Wu, and C. Leighton, Phys. Rev. Lett. **91**, 127202 (2003); J. Wu, J. W. Lynn, C. J. Glinka, J. Burley, H. Zheng, J. F. Mitchell, and C. Leighton, Phys. Rev. Lett. **94**, 037201 (2005); Y. Sun, Y.-K. Tang, and Z.-H. Cheng, cond-mat/0505189.
- ⁶ E. Dagotto, T. Hotta, and A. Moreo, Phys. Rep. **344**, 1 (2001); E. Dagotto, *Nanoscale Phase Separation and Colossal Magnetoresistance*, Springer-Verlag, Berlin, 2002.
- ⁷ T. Motohashi, V. Caignaert, V. Pralong, M. Hervieu, A. Maignan, and B. Raveau, cond-mat/0504379 and references therein.
- ⁸ I. Terasaki, Y. Sasago, K. Uchinokura, Phys. Rev. B **56**, R12685 (1997). See also G. Mahan, B. Sales, and J. Sharp, Physics Today, March 1997, page 42; F. J. Di Salvo, Science **285**, 703 (1999); H. W. Eng, W. Prellier, S. Hebert, D. Grebille, L. Mechin, and B. Mercey, cond-mat/0410177 and references therein.
- ⁹ D. J. Singh, Phys. Rev. B **68**, 020503 (2003).
- ¹⁰ N. Bulut, W. Koshibae, and S. Maekawa, cond-mat/0502347 and references therein.
- ¹¹ M. Mochizuki, Y. Yanase, and M. Ogata, J. Phys. Soc. Jpn. **74**, 1670 (2005) and references therein.
- ¹² M. Ogata, J. Phys. Soc. Jpn. **72**, 1839 (2003); G. Baskaran, Phys. Rev. Lett. **91**, 097003 (2003); B. Kumar and B. S. Shastry, Phys. Rev. B **68**, 104508 (2003) and references therein.
- ¹³ H. Ikeda, Y. Nisikawa, and K. Yamada, J. Phys. Soc. Jpn. **73**, 17 (2004); Y. Nishikawa, H. Ikeda, and K. Yamada, J. Phys. Soc. Jpn. **73**, 1127 (2004).
- ¹⁴ S. R. White, Phys. Rev. Lett. **69**, 2863 (1992).
- ¹⁵ E. Dagotto, Rev. Mod. Phys. **66**, 763 (1994).
- ¹⁶ H. Onishi and T. Hotta, Phys. Rev. B **70**, 100402(R), (2003).
- ¹⁷ Y. Q. Li, M. Ma, D. N. Shi, and F. C. Zhang, Phys. Rev. Lett. **81**, 3527 (1998).
- ¹⁸ B. Frischmuth, F. Mila, and M. Troyer, Phys. Rev. Lett. **82**, 835 (1999).
- ¹⁹ Y. Yamashita, N. Shibata, and K. Ueda, Phys. Rev. B **61**, 4012 (2000).
- ²⁰ C. Itoi, S. Qin, and I. Affleck, Phys. Rev. B **61**, 6747 (2000).
- ²¹ Y. Yamashita, N. Shibata, and K. Ueda, Phys. Rev. B **58**, 9114 (1998).
- ²² H. C. Lee, P. Azaria, and E. Boulat, Phys. Rev. B **69**, 155109 (2005).
- ²³ Actually, it is expected that this exponent $3/2$ will depend on U , J and the density n . Here, we do not intend to present a systematic study of this exponent. Our intention is only to show that at large U , it has the same exponent as the $SU(4)$ model. Note also the similarity with the 1D Hubbard model, where this exponent for $U \rightarrow \infty$ is also $3/2$ (see, for example, J. Voit, Rep. Prog. Phys. **58**, 977 (1995)).
- ²⁴ I. Affleck, Nucl. Phys. **B265**, 409 (1986).
- ²⁵ Note that we tried to calculate directly the finite spin-gap anticipated from the $n=3$ and 4 results. However, this is a difficult task, since even for small systems the spin gap is already very small (less than 10^{-2}).
- ²⁶ F. D. M. Haldane, Phys. Lett. **93A**, 464 (1983); Phys. Rev. Lett. **50**, 1153 (1983).
- ²⁷ M. Ogata and H. Shiba, Phys. Rev. B **41**, 2326 (1990).
- ²⁸ S. Daul and R. M. Noack, Phys. Rev. B **58**, 2635 (1998).
- ²⁹ H. Onishi and T. Hotta, Phys. Rev. B **71**, 180410(R) (2005).